energy&fuels

Fossil Fuels

Effect of tire-char ash on the extent of synergy during CO co-gasification with hydrochar from potassium-rich coconut fiber

Douglas Hungwe, Reza Khoshbouy, Saleem Ullah, Lu Ding, Kunio Yoshikawa, and Fumitake Takahashi

Energy Fuels, **Just Accepted Manuscript** • DOI: 10.1021/acs.energyfuels.0c00895 • Publication Date (Web): 09 Jun 2020

Effect of tire-char ash on the extent of synergy during CO_2 co-gasification with hydrochar from potassium-rich coconut fiber

Douglas Hungwe[1*], Reza Khushbouy[1], Saleem Ullah[2], Ding Lu[3,4*], Kunio Yoshikawa[1], Fumitake Takahashi [1]

1. Tokyo Institute of Technology, 4259 Nagatsuta-cho, Midori-ku, Yokohama, Kanagawa 226-8502, Japan

2. University of Jyväskylä, P.O. Box 35, FI-40014, Finland

3. East China University of Science and Technology, Shanghai 200237, PR China

4. Shanghai Institute of Pollution Control and Ecological Security, Shanghai 200092, P.R. China

Abstract

The influence of inherent tire char ash during co-gasification with coconut hydrochar prepared at different intensities was investigated by thermogravimetric analysis to ascertain the extent to which synergistic interaction, reactivity, and activation energy reduction were altered. High-ash tire tread (TT) and low-ash sidewall (SW) both exhibited enhanced synergy, reactivity, and activation reduction upon co-gasification with hydrochars; however, the extent of promotion was more pronounced in SW-hydrochar blends. This difference was caused by the inhibiting nature of TT inherent ash, particularly the role of Si-containing compounds. Inhibition in TT-hydrochar blends was mainly due to the promotion of alkaline and alkaline earth metal transformation into inactive silicates, and to a lesser extent, the mass transfer effect caused by accumulated ash, especially at conversions higher than 70%. The extent of enhancement correlated well with the concentration of available alkaline and alkaline earth metals. The findings may be useful in justifying the exclusion of high ash tire char as gasification feedstock to mitigate ash-related problems.

1. Introduction

Hitherto, the impetus to reduce dependency on fossil fuels by exploring alternative, green and (or) sustainable energy sources such as biomass,[1,2] waste tire[3,4] and municipal solid waste[5] has intensified, leading to the exploitation of these alternatives in already existing coal-based gasification facilities.[6] However, the commercialization of unary gasification of these candidate fuel-sources is thwarted by several critical fuel quality issues and operational problems. Sole biomass gasification bottlenecks include and are not limited to low bulk and carbon density, high moisture content, mineral matter, irregular morphology, and tar generation.[7,8] Hydrothermal treatment (HT) is one of the pre-treatment methods used to address some of the limitations of biomass utilization, particularly better solid dewatering performance, improving energy density, and homogenization of solid fuel morphology.

Hydrothermal treatment is the thermochemical conversion of biomass into an energy-dense carbonaceous solid using an aqueous medium operated under subcritical conditions.[9,10] The densified solid, also known as hydrochar, is a result of biomass transformation via chemical reactions which include decarboxylation, decarbonylation, dehydration, polymerization, re-condensation, aromatization, and hydrolysis.[1,11] Simultaneously, the process extracts water-soluble ash-forming minerals from biomass into the aqueous phase, thus reducing the alkaline index of resultant hydrochar.[12] Consequently, the tendency for ash fouling and slagging is diminished.[13] Intensive HT conditions can yield chars similar to lignite coal at best, beyond which, more severe conditions render the process uneconomical. Furthermore, the energy density of hydrochar is significantly lower than that of higher rank coals used in gasification facilities, therefore it is imperative to improve the energy density of hydrochar by co-utilization with high calorific carbonaceous material such as waste tire.

Waste tire is an energy-dense (30-40 MJ/kg) carbonaceous material[3] with a heating value higher than that coal.[14] Nascent pyrolytic tire char is relatively inert under CO_2 gasification conditions[6,15] owing to the graphitic structure and a deficiency in reaction-promoting heteroatoms hence requires harsh reaction conditions.[16,17] On the other hand, lignocellulose biomass has ample heteroatoms and catalytic species in the form of alkaline and alkaline earth metals (AAEMs), these are known to significantly improve reactivity.[17–19] Although biomass can greatly improve gasification reactivity, it inevitably produces problematic condensable organic compounds referred to as tar. Tar can be reduced and (or) eliminated by carbonaceous chars,[18] reforming performance is significantly enhanced by doping with transitional metals.[20,21] Zinc-rich tire char is also exploited as an in-situ or ex-situ tar reforming catalyst during co-gasification.[22,23] Co-gasification of biomass and waste tire is therefore complementary because the latter can sequestrate the demerits of the former, and vice versa. A deep understanding of the nature of interactions during co-gasification is, therefore, by no means a trivial matter.

Research on co-gasification of waste tire and biomass has not garnered much attention,[4] to the best of the authors' knowledge only one research group reported on the isothermal and non-isothermal kinetics of CO_2 co-gasification with several biomass residues.[16,17] They confirmed that co-gasification improved process thermodynamics and synergistic interaction, owing to the catalytic role of AAEMs. It is worth mentioning that these previous studies were restricted to one non-specified part of a tire; however, tires are composed of low-ash sidewall (SW) and high-ash tire tread (TT) components. This heterogeneity is not accounted for in co-gasification studies. It follows that the effect of inherent ash on tire-biomass interaction requires investigation to attain a more holistic understanding of synergistic or antagonistic effects during gasification. Our previous study compared the effect of inherent tire ash on the physicochemical evolution of SW and TT char and found that TT formed silica-based ash clusters, which inhibited gasification through

an increase of mass transfer effects and suppression of structural development.[24] SW did not exhibit any inhibition even at near-completion conversion. By inference, such phenomena may have a deleterious effect on co-gasification. For a better understanding of the effect of inherent ash during co-gasification, the mechanism of catalysis requires reviewing.

The proposed mechanism of catalysis is initiated by AAEMs migration from biomass to the tire char. Subsequently, there is deposition and preferential accommodation on and within carbon matrix imperfections resulting in the formation of swelling graphitic intercalation compounds that strain carbon bonds and ease bond breaking.[25,26] In addition, the degree of graphitization[12] and aromatic ring condensation is suppressed,[27] and consequently, the gasification reaction is promoted via a reduction in activation energy. It is, therefore, reasonable to infer that migration and accessibility of the char matrix by catalytic species has a profound effect on the extent and nature of the interaction. High-ash chars can reduce carbon matrix accessibility by intercepting AAEMs and (or) encapsulating the carbon matrix and thus reduce the extent of interaction.[24] Based on this hypothesis, it is worth investigating and quantitatively evaluating the effect of different ash content on synergy or inhibition. Results from such a study are key in justifying the necessity of tire pre-handling protocols to mitigate possible ash-related issues such as incomplete carbon conversion and ash fusion.

In light of this discussion, this paper presents the co-gasification of tire chars of different ash composition with hydrochars from potassium-rich coconut fiber to gain insights on the effect of AAEM concentration on the extent of synergy, reactivity and reduction of activation energy and to delineate the impact of inherent tire ash on the same.

2. Materials and Methods

2.1 Sample Preparation

This section presents the preparation of low-ash tire char, high-ash pyrolytic tire char (TC), and coconut fiber hydrochars.

2.1.1 Hydrochar preparation

Hydrothermal carbonization runs were performed using a 0.5 L batch-type continuously-stirred autoclave reactor (MMJ-500, OM Lab-Tech, Japan). For each run, ~10 g of raw coconut fiber on an as-received basis was mixed with distilled water and charged into the reactor. The mass ratio of coconut fiber (dry basis) to total water was kept at 1:10 for each test. After that, the reactor was purged with argon gas to ensure an inert environment for the carbonization process. Subsequently, the reactor was heated to target temperatures of 180, 200, and 220 °C. The reactor charge was held for 20 min at the target temperature. After each experimental run, the hydrochar was dewatered using a vacuum filter and oven-dried at 105 °C

for 24 h. The hydrochars thus furnished are named HT180, HT200 and HT220, respectively. The chemical analysis of the hydrochars is shown in Table 1.

2.1.2 Tire Sample preparation

The end-of-life tire was separated into SW and TT. The samples were shredded into small pieces (1 cm×1 cm), washed using distilled water to remove impurities and finally air-dried.

2.1.3 Char preparation

Pyrolysis experiments were carried out in an electric reactor; a detailed description of the equipment is reported elsewhere.[28] Chars were prepared in a pyrolysis reactor operated at a temperature of 950°C, and the samples were held for 30 minutes to ensure complete devolatilisation. All samples were ground and sieved to a particle size of less than 105 μm. Pyrolyzed hydrothermally treated coconut fiber prepared at 180, 200, and 220 °C was labeled HT180P, HT200P, and HT220P, respectively. While sidewall and tire tread char is simply tagged SW and TT, respectively.

Table 1. Chemical composition of samples

Sample	HT180	HT200	HT220	TT	SW
			Proximate Analysis (wt%, dry basis)		
Volatiles	76.67	75.36	75.48	0.53	0.69
Fixed Carbon	18.68	21.11	22.32	76.84	89.59
Ash	4.65	3.53	2.20	17.86	3.56
			Ultimate Analysis (wt%, dry ash-free basis)		
C	49.27	51.85	54.25	78.48	92.65
H	5.85	5.56	5.15	1.19	1.05
O [d]	39.98	38.85	38.09	0.42	0.47
N	0.24	0.19	0.30	0.91	1.03
S	0.02	0.01	0.01	1.13	1.24
			XRF Analysis (wt%)		
K_2O	17.92	5.07	1.96	0.92	1.32
SiO_2	27.08	30.81	37.38	52.78	11.21
Na_2O	9.74	2.81	4.12	0.02	0.01
CaO	28.66	38.75	32.58	0.73	6.74
Al_2O_3	6.05	2.22	3.06	1.23	2.66
SO_3	1.19	1.17	1.99	8.69	14.2
MgO	2.67	12.68	11.26	0.42	2.99
Fe_2O_3	0.70	2.62	2.05	1.20	0.91
ZnO	0.10	0.16	0.14	32.84	58.63
	HT180P	HT200P	HT220P	TT	SW
			AAEM concentration (mg/g)		
K	89.60	35.48	12.70	0.25	0.12
Na	25.70	14.05	11.60	0.14	0.20
Ca	20.20	23.10	24.70	0.07	0.06

[d] Calculated by difference.

2.2 Characterization

Feedstock characterization with respect to physicochemical properties is key to explaining and even predicting gasification behavior, particularly chemical composition, ash composition, and degree of carbon disorder.

2.2.1 Chemical and Physical Analysis

Thermogravimetric analysis (Shimadzu DTG- 60H with thermal analyzer TA-60WS, Japan) was used for proximate analysis of all samples, and ultimate analysis was performed using the Vario Micro Cube Elemental Analyzer (Elementary, Japan). Char samples' morphological surface characteristics were determined by scanning electron microscopy (SEM: JSM-6610LA, JEOL Ltd. Japan). The Raman spectra of tire char samples were determined by a NRS-4100 Raman spectroscopy (JASCO, Japan) employing a laser beam of wavelength 532 nm and 1 cm^{-1} resolution. Spectra of wavenumber range 800-2000 cm^{-1} were recorded. The surface area of pyrolyzed chars was measured using an ASAP 2020 analyzer by N_2 gas adsorption method at 77.15 K for pores with a diameter range from 2 nm to 200 nm. The Brunauer–Emmet–Teller (BET) model was used to calculate the specific surface areas of the samples.

2.2.2 Ash Analysis

Ash composition was determined by X-ray fluorescence spectrometry (XRF: S2 Ranger/LE, Bruker AXS, Germany). Only common major constituents existing in both hydrochars and pyrolytic tire chars are presented in Table 1; therefore, the sum of weight percentages is not unity. Water-soluble and ion exchangeable cationic species of pyrolyzed samples were determined using chemical fractionation analysis,[29] and AAEM concentration was measured by an inductively coupled plasma optical emission spectrometer (ICPE-9000, Shimadzu, Japan).

2.3 Gasification Experiments

2.3.1 Experimental Procedure

Char blends were prepared by mixing pyrolytic TC and hydrochar at equal proportions. The blends were labeled accordingly; for example, a mixture of pyrolyzed SW and HT180P was tagged SW-HT180P. Experimental runs were initiated by loading an 8.0 ± 0.5 mg sample in an alumina crucible and heating to a target temperature at 20 °C/min under N_2 (80 mL/min). The sample was held at target temperature for 5 minutes to ensure temperature equilibration; after that, inert gas was switched to high-purity CO_2 (150 mL/min) to initiate gasification. All experiments were done in triplicate. Semichars were prepared by interrupting gasification TGA tests at times corresponding to appropriate conversion, this was achieved by switching CO_2 flow for N_2 to stop the reaction.

2.3.2 Data processing

Raw mass-loss data was converted to conversion-time data by the following equation,

$$x = \frac{m_0 - m_t}{m_0 - m_a} \quad (1)$$

where m_0 is the initial mass of samples, m_t is the instantaneous sample mass at time t and m_a is ash mass. The existence of synergistic/ inhibition effects is determined by comparing non-interactive theoretical conversion and experimental conversion. The theoretical conversion can be calculated according to Equation 2;[30]

$$x_{cal} = \frac{F_{TC}\left(m_{TC,0} - m_{TC,t}\right) + F_{HT}\left(m_{HT,0} - m_{HT,t}\right)}{F_{TC}\left(m_{TC,0} - m_{TC,a}\right) + F_{HT}\left(m_{HT,0} - m_{HT,a}\right)} \quad (2)$$

where F_{TC} and F_{HT} is tire char and hydrochar mass fractions in the blended chars, respectively.

2.3.3 Determination of Activation Energy

The activation energy can be obtained by using an isoconversional method[31] and the derivation is presented below. The rate law is given by;

$$r = \frac{dx}{dt} = k(T) f(x) \quad (3)$$

where $f(x)$ is a mathematical expression of a suitable reaction model, $k(T)$ is the rate constant at temperature T. The reaction rate expressed as a function of temperature is described by the Arrhenius equation given by;

$$k = k_0 e^{-\left(\frac{E_A}{RT}\right)} \quad (4)$$

where E_A is the activation energy (J/mol), k_0 is the frequency factor in min^{-1}, R is the ideal gas constant $(8.314\ J/mol\ K)$, T is temperature in kelvin.

Equation 3 is solved by integration of separated variables;

$$\int_0^x \frac{dx}{f(x)} = G(x) = k_x(T) t_x(T) \quad (5)$$

where k_x and t_x is the rate constant (min^{-1}) and residence time (min) at a specific conversion x. Combining equations 4 and 5 and solving yields

$$\ln\left[t_x(T)\right] = \alpha + \frac{E_A}{RT} \quad (6)$$

where $\alpha = \ln G(x) - lnk_0$, is a constant at a specified conversion. The activation energy is calculated from the gradient of ln (t_x) against 1/T plots at varying conversion levels.

3. Results and Discussion

3.1 Sample characterization

The proximate, XRF, and chemical fractionation analysis of hydrochars shows that the severity of hydrothermal treatment conditions increases fixed carbon content and reduces ash content, mostly water-soluble species.

Scanning electron microscopy micrographs of pyrolyzed raw coconut fiber and hydrochars are shown in Figure 1, demonstrate the morphological changes associated with the combined effect of the severity of HT conditions and pyrolysis. The longitudinal section of the raw fiber is characterized by a filamentous morphology with a relatively smooth epidermis on which there are nearly-even distributed globular protrusions. The cross-sectional area is xylem composed of a honeycombed-shaped network with hollow channels. Pyrolytic HT180 suggests that HT erodes or facilitates the erosion of protrusions resulting in pits on the fiber surface, while the inner skeletal morphology does not exhibit considerable change. It is reasonably inferred that the protrusions are composed of non-refractory biomass components such as extractives and hemicellulose.

As the HT conditions intensified, the pits were transformed into parallel reticulate micro-ridges that run parallel to strand length, leaving behind an open-structured HT recalcitrant xylem skeletal core, as shown in Figure 1 (d). Nitrogen adsorption test results show that pyrolyzed hydrochars have a well-developed porous structure. The surface area of the pyrolytic HT180P, HT200P, and HT220P chars is 312.7 m^2/g, 324.9 m^2/g, and 365.2 m^2/g, respectively. Figure 1 (e-f) shows the surface morphology of pyrolytic SW and TT. The SW is characterized by a smooth surface with no perceivable degree of defects or porosity, while TT has a relatively rough surface. The presence of silica-based ash clusters causes surface roughness. Detailed ash characterization is reported elsewhere.[24] The surface area of the tire chars is 53.6 m^2/g and 30.5 m^2/g for TT and SW, respectively. Similar results were reported in our previous work,[24] however, the surface area in this study is much lower; the reason is that a different tire brand was used. It should be remarked that tire char is meso/macroporous solid, [32,33] implying that premature pore coalescence during gasification, thus inhibiting the reaction through a reduction in available surface area. The surface area of chars is dependent on the type of carbon black used during tire manufacture. For example, common

commercial carbon blacks, N660, NCB, and HCB have a surface area of 35.75 m^2/g, 80.08 m^2/g, and 138.90 m^2/g.[32]

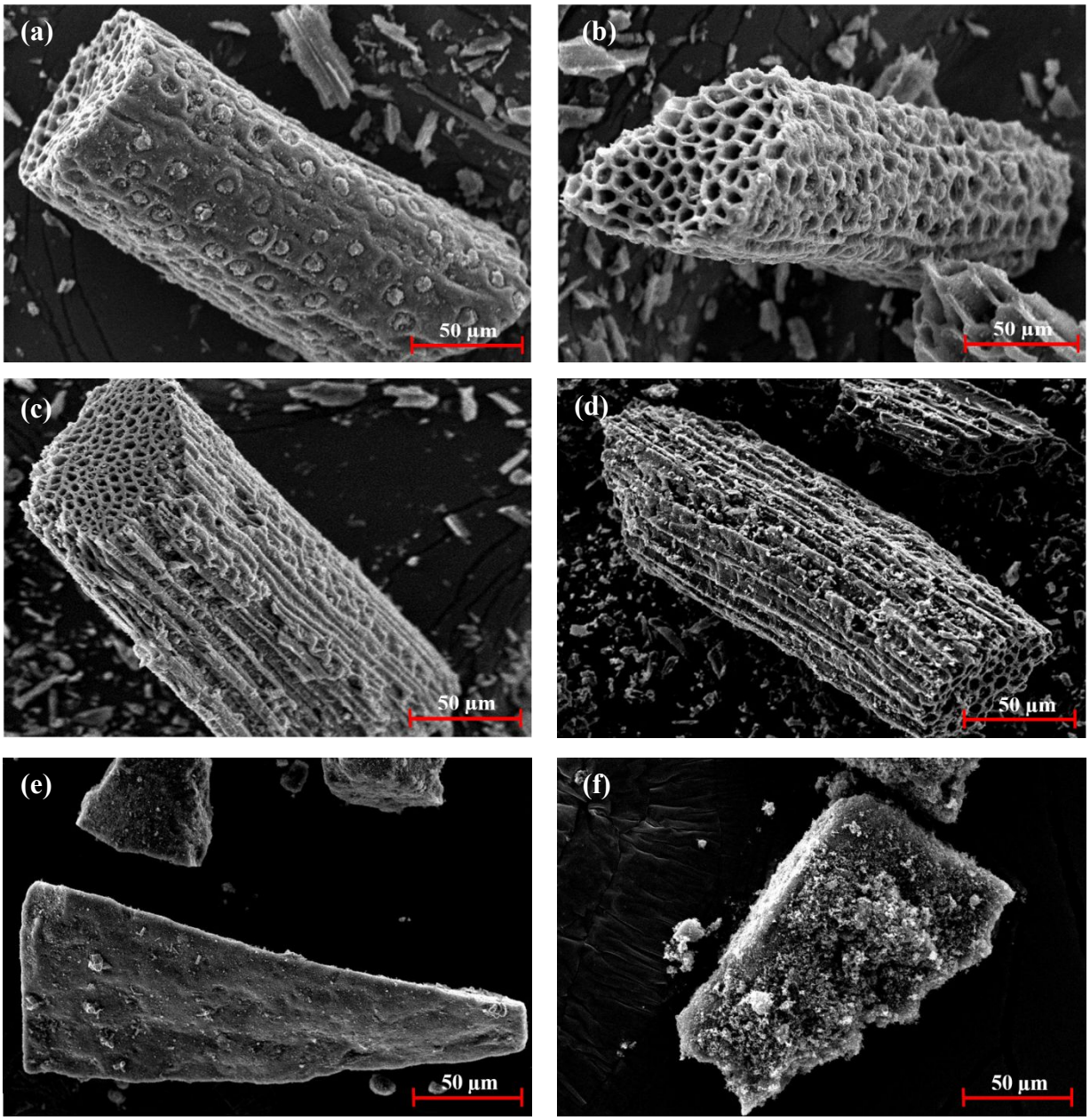

Figure 1. SEM images of pyrolytic samples. (a)raw coconut fiber (b) HT180 (c) HT200 (d) HT220 (e) SW (f)TT

3.2 Influence of inherent tire ash on gasification characteristics

Preliminary gasification tests with 10±0.5 mg samples were conducted to investigate the effect of ash on gasification, and to emphasize and make clear the distinct reaction profiles of tire char caused by a

difference in ash content. The TT and SW CO_2 gasification profiles of chars are superimposed on each other and presented in Figure 2.

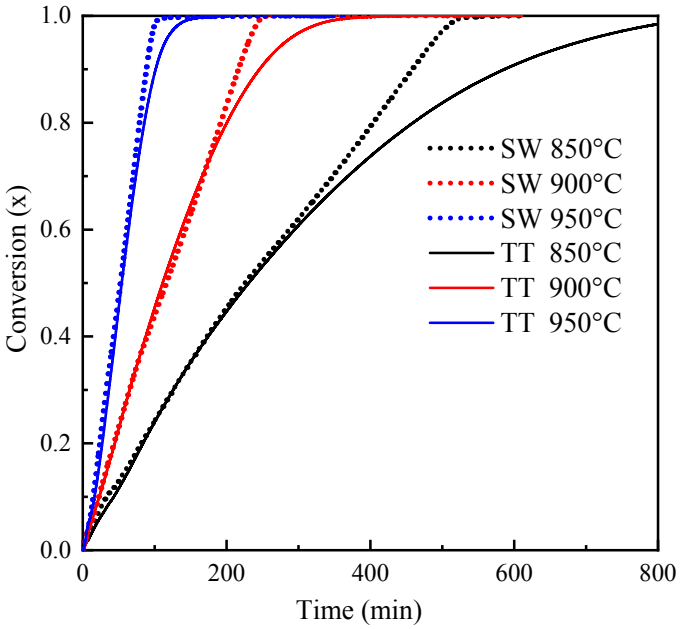

Figure 2. Conversion-time profiles of tire char

Line graphs indicate that the effect of ash is inconsequential at conversions averaging below 70% despite the significant difference in ash content and composition. It is observed that the profiles are coincident up to nearly 70% conversion at all temperatures, suggesting that the reactivity is similar within that range. The coincidence can be explained by considering the chemical composition of waste tire rubber.

Waste tire rubber (by order of abundance and excluding steel/fabric reinforcement) is comprised of carbon black, natural rubber, synthetic rubber, and mineral matter.[34,35] During pyrolysis, most, if not all, of the rubber is expelled as volatiles, leaving behind an ash-laden carbon-black-rich char with minor proportions of entrapped rubber remnants/deposits.[33] Therefore, tire pyrolysis can be considered a carbon black enriching or recovery process.[36] For this reason, it is reasonable to infer that the coincidence of the conversion profiles is a consequence of the reaction of the most dominant component of tire char, carbon black. Deviation from coincidence at higher conversions is attributed to the inhibiting nature of residual ash in the fixed bed, particularly silica-based ash clusters. A linear profile characterizes SW, while TT has a linear trend at lower conversions and a protracted profile at higher conversions. The effect of inherent ash is quantitatively evaluated by comparing the reaction times of these chars. In contrast to SW char, the reaction time of TT is increased by a factor of 1.58, 1.72, and 1.86 times at temperatures 850, 900, and 950°C because of mass transfer resistance imposed by the presence of silica-laden ash. Conversion profile coincidence also suggests that ash components act as spectator inorganic species; some researchers[37]

reported that tire char is mostly comprised of acid-leachable (at elevated temperature) inorganic species, which implies inactivity during gasification. Only water-soluble and ion-exchangeable inorganic AAEMs are reported to affect gasification positively through catalysis.[38,39] For TT char, the char-ash transition for conversion less than 70% is described by the shrinking particle model, within which the carbon structure is the dominant factor, while at a later stage, transition model changes to the shrinking particle core model as the effect of accumulated ash gradually takes a more significant role.[24,40] The SW char can only be described by the shrinking particle model owing to the low content of ash.[24] To ensure that only the influence of ash is studied, the chemical structure of carbon in TT and SW char has to be the same. For this reason, the chemical structure of tire chars was determined using Raman spectroscopy.

As presented in Figure 3, both chars are characterized by two shifts at ~1350 cm^{-1} and ~1600cm^{-1}, these are referred to as D-band and G-band, respectively. The D-band represents structural defects and disorder in the carbon structure derived from sp^3 carbon vibrations, while the G-band represents a graphitic crystalline structure related to sp^2 carbon vibrations.[41] The intensity of the G-band is higher than that of the D-band, indicating a high degree of graphitization and a lack of structural defects; this explains the low reactivity of tire char. Visually, the two spectra suggest a similar structure in TT and SW, therefore the spectra were deconvoluted to evaluate individual band intensities quantitatively. The results are shown in Table 2. The intensity ratio I_G/I_{all} was used to evaluate the carbon ordering degree of chars,[42] a high value of the intensity ratio indicates a degree of graphitization.

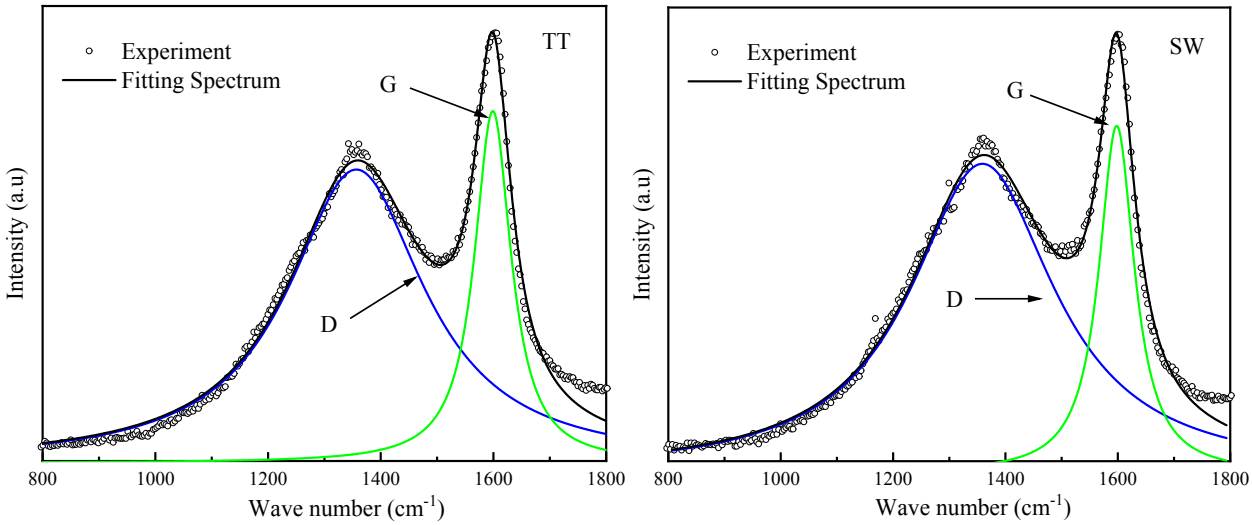

Figure 3. Raman spectra for tire tread and sidewall char

It was found that the order degree for both chars is 0.230±0.014, with SW char exhibiting a slightly higher graphitization degree. Considering char compositions discussed hereinabove and the same thermal history

of the chars, the slight variation may be due to the varying extents to which nascent pyrolytic chars expel or retain repolymerization products owing to the role of initial mineral matter.

Table 2. Microstructure Parameters of Tire Char

sample	I_D	I_G	I_G/I_{all}
TT char	284	78.3	0.216
SW char	253	81.3	0.243

To corroborate this speculation, one study[36] reported that pyrolytic tire char recovered for high-temperature pyrolysis is predominantly mineral-rich carbon black with carbonaceous deposits on its surface. The high surface area in TT char could imply more accommodation of these deposits and hence a lower degree of graphitization, as reflected in Table 2. Based on this analysis and discussion, the chemical structure of chars can be considered to be the same since the effect on gasification reactivity is slight, as demonstrated by the coincidence of SW and TT char gasification profiles.

3.3 The effect of blending on tire char reactivity

Gasification reactivity curves of individual and blended char samples are shown in Figure 4. Figure 5 shows the extent of gasification enhancement when tire char is blended with hydrochars.

The gasification reactivity was quantitatively evaluated by the reactivity index ($R_{0.9}$) in h^{-1}, which is calculated as follows:[43]

$$R_{0.9} = \frac{0.9}{t_{0.9}} \tag{7}$$

where $t_{0.9}$ is the gasification time needed to reach char conversion of 0.9.

It is observed that the reactivity of TT is much lower than that SW char, owing to the inhibiting nature inherent ash. Generally, the blending of tire char with hydrochar improved the reactivity of tire char. The trend of reactivity for SW and SW-hydrochar blends is; SW-HT180P > SW-HT200P > SW-HT220P > SW. The same trend was observed for TT and TT-hydrochar blends. This trend correlates well with the available AAEMs concentration in hydrochars. It is observed that HT180 has the highest enhancement effect on reactivity. The order of hydrochar reactivity enhancement follows the trend; HT180P > HT200P > HT220P. The high reactivity enhancement capacity of hydrochars emanates from the role of AAEMs. The low reactivity of tire chars is due to the low available micropore surface area, high graphitic crystalline structure, and the presence of a high concentration of acidic mineral content.

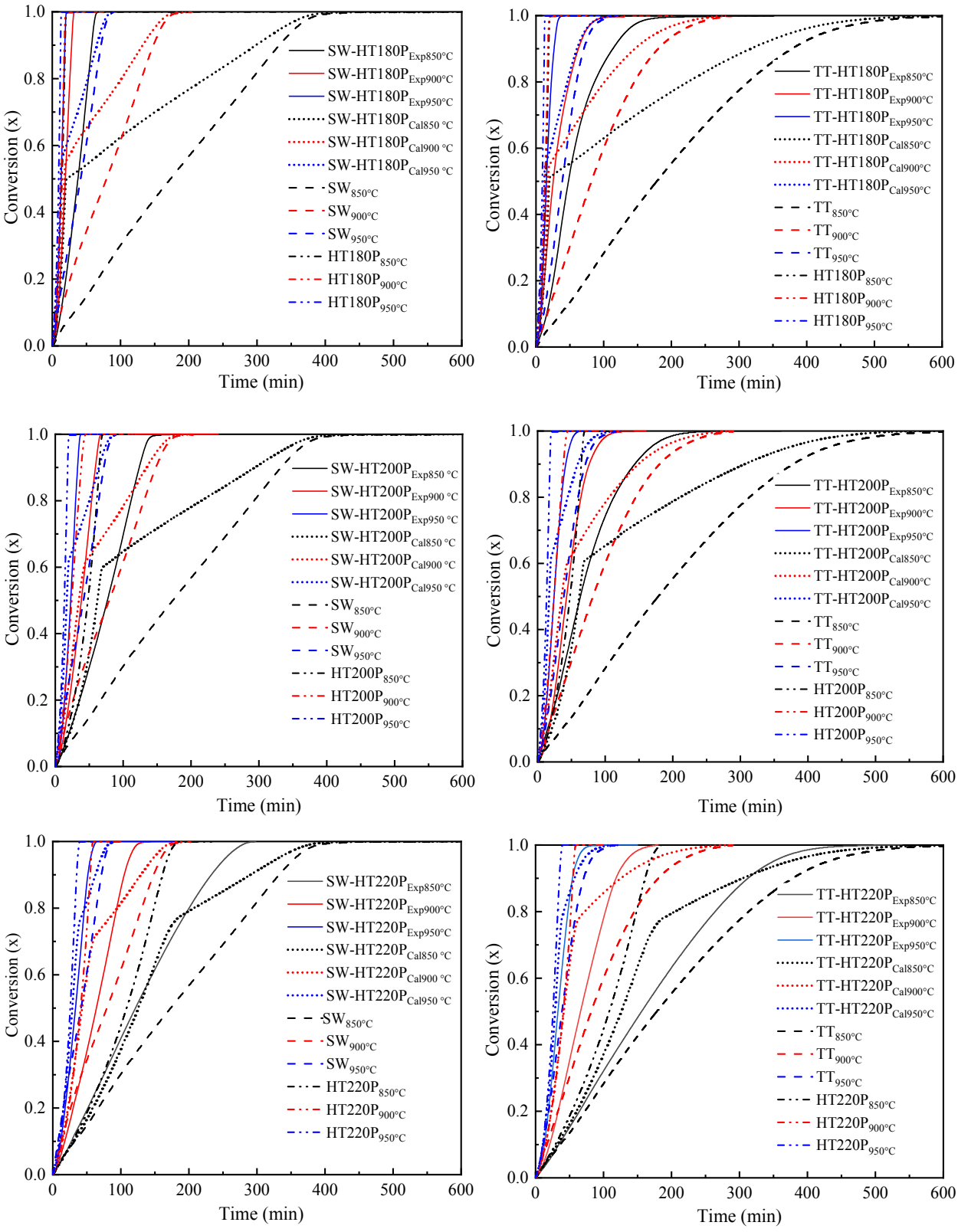

Figure 4. Gasification reactivity curves of tire char and tire-hydrochar blends

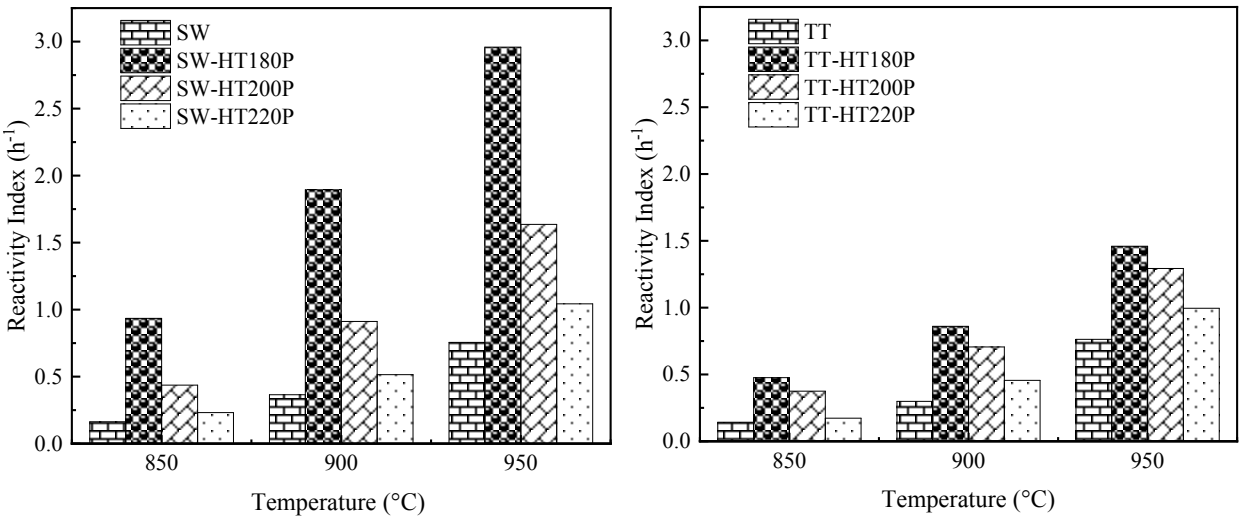

Figure 5. Effect of blending on reactivity

The addition of hydrochars to tire chars significantly improves gasification performance. The promotional effect of elevated temperature on gasification is demonstrated in the same figure. For example, when the gasification temperature is increased from 850 to 950°C, the reactivity of SW-HT180P triples. The same figure illustrates that the extent of enhancement for SW is more pronounced compared to TT owing to the difference in ash content highlighted above. It is reasonable to infer that the inherent tire ash has an inhibiting influence on reactivity enhancement since the magnitude of reactivity indices of TT-hydrochar blends is much lower compared to SW blends.

3.4 Effect of blending on synergy

Reactivity curves shown in Figure 4 have experimental and calculated reactivity curves. Calculated reactivity curves are a result of combining individual reactivity curves of tire char and hydrochar, according to equation 2. Synergistic behavior or inhibition is derived from comparing experimental and calculated reactivity curves. When the latter is higher than the former, it means there is synergistic interaction, and when the former is higher than the latter, inhibition is confirmed. A special case exists when the two curves are coincident, in which case non-interaction exists.

The synergy factor was calculated to determine the nature of interaction according to the equation;[44]

$$Synergy\ factor = \frac{R_{0.9,\exp}}{R_{0.9,cal}} \qquad (8)$$

where $R_{0.9,cal}$ and $R_{0.9,\exp}$ denotes calculated and experimental reactivity, respectively. Figure 6 shows the effect of blending on the synergy factor.

The primary interaction mechanism between tire char and hydrochar was found to be the synergistic effect. Blends with SW char exhibited a stronger synergistic effect compared to TT containing blends. At all temperatures, the trend for synergy for all chars followed the trend; TC-HT180P > TC-HT200P > TC-220P. This trend has a strong correlation with the availability of AAEMs.

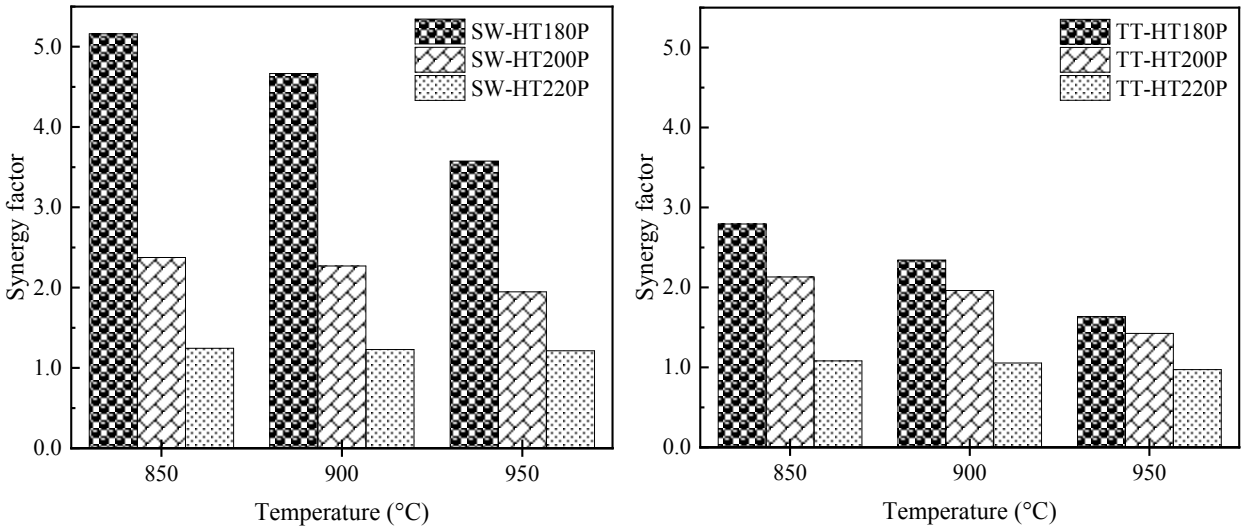

Figure 6. Effect of blending on synergy

Interestingly, when tire chars are blended with the same hydrochar, the SW blends show a significantly higher synergy factor. This observation implies that acidic ash decreases the extent of synergy. The extent of synergy enhancement in the case of HT220P is not significant compared to HT180P and HT200P owing to low AAEM concentration and possibly deactivation thereof. An increase in temperature is marked by a decrease in the synergy factor owing to the promotion of internal and external AAEMs deactivation reaction with silica and alumina minerals. On the basis of these findings, it is concluded that an increase in AAEMs concentration promotes synergy, while an increase in temperature or acidic ash concentration hampers synergistic interaction.

The apparent negative effect of accumulated ash on tire reactivity at conversions higher than 70% is discussed hereinabove, and it is, therefore, necessary to explore the effect thereof on activation energy reduction since AAEMs are known to catalyze gasification reactions. Only conversions greater than 70% are considered in a bid to elucidate the effect of accumulated ash on co-gasification.

3.5 Effect of blending on activation energy reduction

It was established that ash accumulation at high conversion causes a protracted gasification time for TT; it follows that initiating and maintaining the gasification reaction becomes more energy-intensive as the reaction reaches near-completion. The effect can be observed by calculating the fractional observed

activation energy of chars during gasification calculated according to the isoconversion method.[31] The same approach can be used to determine the extent to which activation energy is altered when tire char is blended.

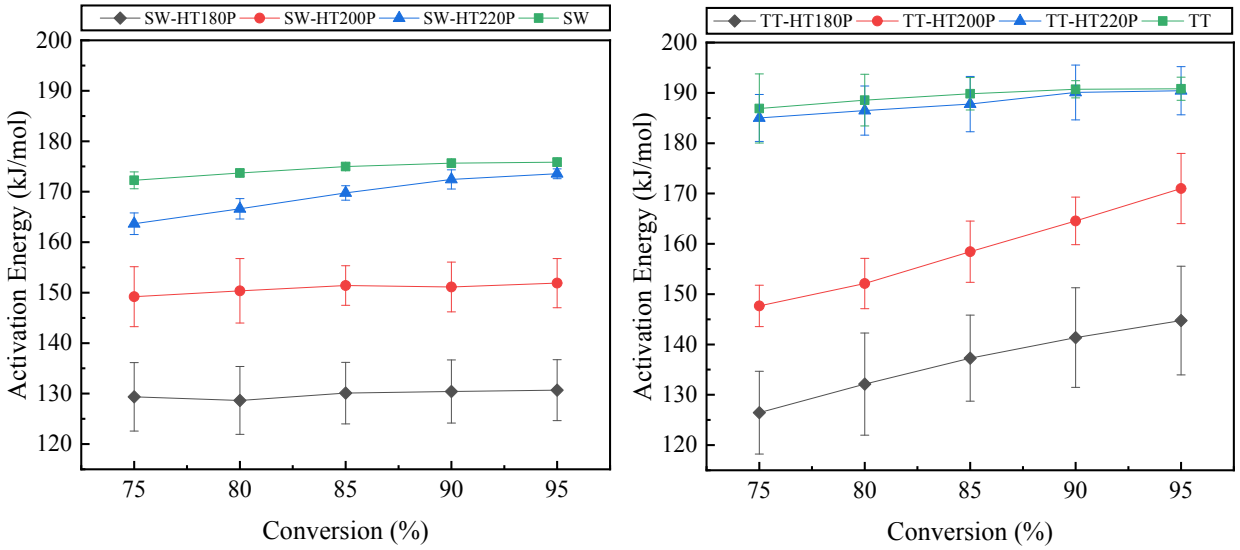

Figure 7. Effect of blending and conversion on activation energy

The observed activation energy of TT and SW between the conversion range 75-95% averages between 189 and 175 kJ/mol, respectively. Blending tire char and hydrochar reduced the activation energy in all blends; however, the change for TT-HT220P is negligible, as illustrated in Figure 7. This implies that the HT220P AAEMs concentration is not adequate to pose a significant catalytic effect for TT; on the contrary, SW-HT220P activation energy reduced to a range much lower compared to the former. At conversions greater than 75%, there is a significant accumulation of Si-containing ash, which increases with reaction progress, and as such, the negative effect of ash becomes more prominent. The steeper gradient exhibited by TT-HT200P is attributable to the extent of AAEMs deactivation relative to the initial concentration of AAEMs since TT-HT200P is less than TT-HT180P. It is reasonable to infer that, for TT-HT200P, a relatively greater proportion of AAEMs is immobilized and deactivated before accessing the carbon matrix, while TT-HT180 may have more available AAEMs even after experiencing the same extent of deactivation as the former. Furthermore, the higher concentration of AAEMs may result in suppressing carbon graphitization, thus decreasing the observed activation energy of the gasification reaction.

These observations suggest that TT ash inhibits carbon matrix accessibility via mass transfer effects and (or) AAEMs transformation into inactive AAEM-aluminosilicates or silicates. By extension, comparison with SW-HT220P reveals that inherent ash inhibition is not pronounced because of the low ash content. The change in activation energy with respect to conversion for SW-HT180P and SW-HT200P shows that blending reduced the observed activation energy of SW to an average of 130 and 151 kJ/mol, respectively. The nearly horizontal trend implies the absence of any significant inhibition effects. On the

contrary, TT-HT180P and TT-HT200P observed activation energy ranges are 126 -145 kJ/mol and 148-171 kJ/mol, respectively. A positive gradient characterizes the change in activation for TT-hydrochar blends, as illustrated in Figure 7. This case confirms the presence of noticeable inhibition effects associated with a significant amount of acidic tire ash. The degree of activation energy reduction for all blended samples follows the trend; TC-HT180P > TC-HT200P > TC-HT220P. The trend has a good correlation with the concentration of AAEMs.

Interestingly, the trend for observed activation for tire blends with HT180P and HT200P show a good correlation with conversion-time profiles of tire char, which is near-coincidence at low conversions and divergence at higher conversions. This observation further demonstrates the negative effect of tire ash on co-gasification, and it is reasonable to infer that inhibition is a combination of mass transfer effects caused by ash accumulation and possibly a decrease in matrix accessibility by physical interception and (or) AAEMs deactivation. Further analysis was conducted to confirm the presence and degree of AAEMs transformation exhibited by different tire chars.

Tire blends with HT200P were gasified at 950°C and interrupted at 90% conversion to evaluate the degree of deactivation. The gasification temperature of 950°C was selected because the temperature in this range promotes AAEM transformation into non-active species such as alkaline metal-aluminosilicates and silicates.[5] The results are summarized in Table 3.

Table 3. AAEM concentration of blended pristine chars and semichars

samples	AAEM concentration (mg/g)		
	K	Na	Ca
TT-HT200P	17.87	7.10	11.59
TT-HT200P-90-950°C	3.12	1.03	3.27
SW-HT200P	17.80	7.13	11.58
SW-HT200P-90-950°C	3.22	1.22	9.11

Note: TC-HT200P-90-950°C is semi-char (conversion, 0.9) of TC-HT200P gasified at temperature of 950°C

Initial total AAEM concentration of blends is almost equal; however, after gasification up to 90% conversion, the concentration is reduced to a much higher degree for TT than SW. It should be noted that alkaline metals are released from char at temperatures higher than 850°C,[45,46] while calcium is retained in the char or semichar during gasification.[5] For this reason, experimental results of potassium and sodium are considered as volatilized inorganics owing to elevated temperature. To corroborate the veracity of this reasoning, the two semichars constituting high and low-ash tire char has at least 82% reduction of alkaline metals, although ash content is different. This confirms that ash behavior other than alkaline deactivation is at play; therefore, only calcium species were considered for semi-quantitative determination of the extent

of deactivation through the reaction with silica and alumina. Furthermore, there is a preferential reaction of calcium with silica compared to sodium and potassium.[47]

In the SW-HT200P blend, calcium content reduced by 21%, while TT-HT200P blend reduced by 72%, confirming the negative effect of TT silica-rich ash on co-gasification. These findings confirm deactivation as one of the mechanisms through which the capability of hydrochar to decrease tire char activation energy is reduced. The same can be used as a measure of interception since catalyst species are immobilized and prevented from accessing residual carbon structure through migration.

It should be noted that the deactivation levels may be higher than the actual levels because of the tendency of AAEMs species to stick to the alumina pan surface; however, the findings are still useful for a comparative study and should be strictly treated as apparent values. Nevertheless, the negative impact of inherent tire ash is adequately demonstrated.

4. Conclusion

Tire chars of different ash compositions were co-gasified with hydrochars from potassium-rich coconut fiber to gain insights on the effect of AAEM concentration on the extent of synergy, reactivity, and reduction of activation energy. A high concentration of AAEMs enhanced reactivity, synergistic effects, and the degree of activation energy reduction. An increase in temperature promoted reactivity because of the endothermic nature of gasification reactions; in contrast, synergy decreased owing to the promotion of AAEMs transformation at elevated temperatures. The extent of enhancement for all the factors mentioned above was more pronounced for SW compared to TT, owing to the inhibiting nature of TT inherent ash. Additionally, inhibition in TT was mainly due to the high concentration of acidic ash, particularly Si-containing minerals, which acts as a site of AAEMs deactivation and, to a lesser extent, the mass transfer effect caused by accumulated ash. It may be prudent to exclude the tire tread from the tire when considering co-gasification as it may result in high catalyst consumption and unreacted carbon, thus reducing reactor efficiency.

Author Information

Corresponding Author

Tel: +81-45-924-5507. Fax: +81-45-924-5518, E-mail: Douglas Hungwe hungwe.d.aa@m.titech.ac.jp, doughungwe@gmail.com and Lu Ding dinglu@ecust.edu.cn

Acknowledgment

This study was supported financially by JSPS KAKENHI Grant Number 18H01567. The authors appreciate Suzukakedai & Ookayama Materials Analysis Division, Technical Department, Tokyo Institute of Technology, for SEM, XRF and Raman Spectroscopy analysis. Contribution from Lonah J. Mikonga is deeply appreciated.

References

(1) Fang, J.; Zhan, L.; Ok, Y. S.; Gao, B. Minireview of Potential Applications of Hydrochar Derived from Hydrothermal Carbonization of Biomass. *J. Ind. Eng. Chem.* **2018**. https://doi.org/10.1016/j.jiec.2017.08.026.

(2) Shen, Y.; Fu, Y. Advances in: In Situ and Ex Situ Tar Reforming with Biochar Catalysts for Clean Energy Production. *Sustain. Energy Fuels* **2018**, *2* (2), 326–344. https://doi.org/10.1039/c7se00553a.

(3) Czajczyńska, D.; Krzyżyńska, R.; Jouhara, H.; Spencer, N. Use of Pyrolytic Gas from Waste Tire as a Fuel: A Review. *Energy* **2017**. https://doi.org/10.1016/j.energy.2017.05.042.

(4) Oboirien, B. O.; North, B. C. A Review of Waste Tyre Gasification. *J. Environ. Chem. Eng.* **2017**, *5* (5), 5169–5178. https://doi.org/10.1016/j.jece.2017.09.057.

(5) Wei, J.; Guo, Q.; He, Q.; Ding, L.; Yoshikawa, K.; Yu, G. Co-Gasification of Bituminous Coal and Hydrochar Derived from Municipal Solid Waste: Reactivity and Synergy. *Bioresour. Technol.* **2017**, *239*, 482–489. https://doi.org/10.1016/j.biortech.2017.05.014.

(6) Straka, P.; Bučko, Z. Co-Gasification of a Lignite/Waste-Tyre Mixture in a Moving Bed. *Fuel Process. Technol.* **2009**. https://doi.org/10.1016/j.fuproc.2009.05.021.

(7) Fermoso, J.; Arias, B.; Gil, M. V.; Plaza, M. G.; Pevida, C.; Pis, J. J.; Rubiera, F. Co-Gasification of Different Rank Coals with Biomass and Petroleum Coke in a High-Pressure Reactor for H2-Rich Gas Production. *Bioresour. Technol.* **2010**. https://doi.org/10.1016/j.biortech.2009.12.035.

(8) Rizkiana, J.; Guan, G.; Widayatno, W. B.; Hao, X.; Huang, W.; Tsutsumi, A.; Abudula, A. Effect of Biomass Type on the Performance of Cogasification of Low Rank Coal with Biomass at Relatively Low Temperatures. *Fuel* **2014**. https://doi.org/10.1016/j.fuel.2014.06.008.

(9) He, C.; Giannis, A.; Wang, J. Y. Conversion of Sewage Sludge to Clean Solid Fuel Using Hydrothermal Carbonization: Hydrochar Fuel Characteristics and Combustion Behavior. *Appl. Energy* **2013**. https://doi.org/10.1016/j.apenergy.2013.04.084.

(10) Mumme, J.; Eckervogt, L.; Pielert, J.; Diakité, M.; Rupp, F.; Kern, J. Hydrothermal Carbonization of Anaerobically Digested Maize Silage. *Bioresour. Technol.* **2011**. https://doi.org/10.1016/j.biortech.2011.06.099.

(11) Fakkaew, K.; Koottatep, T.; Polprasert, C. Effects of Hydrolysis and Carbonization Reactions on Hydrochar Production. *Bioresour. Technol.* **2015**. https://doi.org/10.1016/j.biortech.2015.05.091.

(12) Mosqueda, A.; Wei, J.; Medrano, K.; Gonzales, H.; Ding, L.; Yu, G.; Yoshikawa, K. Co-Gasification Reactivity and Synergy of Banana Residue Hydrochar and Anthracite Coal Blends. *Appl. Energy* **2019**. https://doi.org/10.1016/j.apenergy.2019.05.008.

(13) Yang, M.; Xie, Q.; Wang, X.; Dong, H.; Zhang, H.; Li, C. Lowering Ash Slagging and Fouling Tendency of High-Alkali Coal by Hydrothermal Pretreatment. *Int. J. Min. Sci. Technol.* **2019**, *29*

(3), 521–525. https://doi.org/10.1016/j.ijmst.2018.05.007.

(14) Portofino, S.; Donatelli, A.; Iovane, P.; Innella, C.; Civita, R.; Martino, M.; Matera, D. A.; Russo, A.; Cornacchia, G.; Galvagno, S. Steam Gasification of Waste Tyre: Influence of Process Temperature on Yield and Product Composition. *Waste Manag.* **2013**. https://doi.org/10.1016/j.wasman.2012.05.041.

(15) Lee, J. S.; Kim, S. D. Gasification Kinetics of Waste Tire-Char with CO2 in a Thermobalance Reactor. *Energy* **1996**, *21* (5), 343–352. https://doi.org/10.1016/0360-5442(95)00119-0.

(16) Lahijani, P.; Zainal, Z. A.; Mohamed, A. R.; Mohammadi, M. Co-Gasification of Tire and Biomass for Enhancement of Tire-Char Reactivity in CO2 Gasification Process. *Bioresour. Technol.* **2013**, *138*, 124–130. https://doi.org/10.1016/j.biortech.2013.03.179.

(17) Lahijani, P.; Mohammadi, M.; Mohamed, A. R. Investigation of Synergism and Kinetic Analysis during CO2 Co-Gasification of Scrap Tire Char and Agro-Wastes. *Renew. Energy* **2019**, *142*, 147–157. https://doi.org/10.1016/j.renene.2019.04.113.

(18) Shen, Y. Chars as Carbonaceous Adsorbents/Catalysts for Tar Elimination during Biomass Pyrolysis or Gasification. *Renewable and Sustainable Energy Reviews*. 2015. https://doi.org/10.1016/j.rser.2014.11.061.

(19) Shen, Y.; Zhao, P.; Shao, Q.; Ma, D.; Takahashi, F.; Yoshikawa, K. In-Situ Catalytic Conversion of Tar Using Rice Husk Char-Supported Nickel-Iron Catalysts for Biomass Pyrolysis/Gasification. *Appl. Catal. B Environ.* **2014**, *152–153* (1), 140–151. https://doi.org/10.1016/j.apcatb.2014.01.032.

(20) Shen, Y.; Zhao, P.; Shao, Q.; Ma, D.; Takahashi, F.; Yoshikawa, K. In-Situ Catalytic Conversion of Tar Using Rice Husk Char-Supported Nickel-Iron Catalysts for Biomass Pyrolysis/Gasification. *Appl. Catal. B Environ.* **2014**. https://doi.org/10.1016/j.apcatb.2014.01.032.

(21) Shen, Y.; Zhao, P.; Shao, Q.; Takahashi, F.; Yoshikawa, K. In Situ Catalytic Conversion of Tar Using Rice Husk Char/Ash Supported Nickel-Iron Catalysts for Biomass Pyrolytic Gasification Combined with the Mixing-Simulation in Fluidized-Bed Gasifier. *Appl. Energy* **2015**. https://doi.org/10.1016/j.apenergy.2014.10.074.

(22) Zhou, Q.; Zarei, A.; De Girolamo, A.; Yan, Y.; Zhang, L. Catalytic Performance of Scrap Tyre Char for the Upgrading of Eucalyptus Pyrolysis Derived Bio-Oil via Cracking and Deoxygenation. *J. Anal. Appl. Pyrolysis* **2019**, *139*, 167–176. https://doi.org/10.1016/J.JAAP.2019.02.001.

(23) Al-Rahbi, A. S.; Williams, P. T. Hydrogen-Rich Syngas Production and Tar Removal from Biomass Gasification Using Sacrificial Tyre Pyrolysis Char. *Appl. Energy* **2017**, *190*, 501–509. https://doi.org/10.1016/J.APENERGY.2016.12.099.

(24) Hungwe, D.; Ding, L.; Khoshbouy, R.; Yoshikawa, K.; Takahashi, F. Kinetics and Physicochemical Morphology Evolution of Low and High-Ash Pyrolytic Tire Char during CO2 Gasification. *Energy and Fuels* **2020**, *34* (1), 118–129. https://doi.org/10.1021/acs.energyfuels.9b03043.

(25) Lahijani, P.; Zainal, Z. A.; Mohammadi, M.; Mohamed, A. R. Conversion of the Greenhouse Gas CO2 to the Fuel Gas CO via the Boudouard Reaction: A Review. *Renewable and Sustainable Energy Reviews*. 2015. https://doi.org/10.1016/j.rser.2014.08.034.

(26) Zhang, Y.; Zheng, Y.; Yang, M.; Song, Y. Effect of Fuel Origin on Synergy during Co-Gasification of Biomass and Coal in CO2. *Bioresour. Technol.* **2016**. https://doi.org/10.1016/j.biortech.2015.10.076.

(27) Tay, H.-L.; Kajitani, S.; Wang, S.; Li, C.-Z. A Preliminary Raman Spectroscopic Perspective for

the Roles of Catalysts during Char Gasification. *Fuel* **2014**, *121*, 165–172. https://doi.org/10.1016/J.FUEL.2013.12.030.

(28) Hardi, F.; Imai, A.; Theppitak, S.; Kirtania, K.; Furusjö, E.; Umeki, K.; Yoshikawa, K. Gasification of Char Derived from Catalytic Hydrothermal Liquefaction of Pine Sawdust under a CO2 Atmosphere. *Energy and Fuels* **2018**, *32* (5), 5999–6007. https://doi.org/10.1021/acs.energyfuels.8b00589.

(29) Chen, H.; Chen, X.; Qiao, Z.; Liu, H. Release and Transformation Characteristics of K and Cl during Straw Torrefaction and Mild Pyrolysis. *Fuel* **2016**. https://doi.org/10.1016/j.fuel.2015.11.059.

(30) Wei, J.; Guo, Q.; Gong, Y.; Ding, L.; Yu, G. Synergistic Effect on Co-Gasification Reactivity of Biomass-Petroleum Coke Blended Char. *Bioresour. Technol.* **2017**. https://doi.org/10.1016/j.biortech.2017.03.010.

(31) Gomez, A.; Mahinpey, N. A New Method to Calculate Kinetic Parameters Independent of the Kinetic Model: Insights on CO2 and Steam Gasification. *Chem. Eng. Res. Des.* **2015**, *95*, 346–357. https://doi.org/10.1016/j.cherd.2014.11.012.

(32) Wang, M.; Zhang, L.; Li, A.; Irfan, M.; Du, Y.; Di, W. Comparative Pyrolysis Behaviors of Tire Tread and Side Wall from Waste Tire and Characterization of the Resulting Chars. *J. Environ. Manage.* **2019**, *232* (July 2018), 364–371. https://doi.org/10.1016/j.jenvman.2018.10.091.

(33) Murillo, R.; Navarro, M. V.; López, J. M.; García, T.; Callén, M. S.; Aylón, E.; Mastral, A. M. Activation of Pyrolytic Tire Char with CO2: Kinetic Study. *J. Anal. Appl. Pyrolysis* **2004**, *71* (2), 945–957. https://doi.org/10.1016/j.jaap.2003.12.005.

(34) Siddique, R.; Naik, T. R. Properties of Concrete Containing Scrap-Tire Rubber - An Overview. *Waste Manag.* **2004**, *24* (6), 563–569. https://doi.org/10.1016/j.wasman.2004.01.006.

(35) Li, G.; Stubblefield, M. A.; Garrick, G.; Eggers, J.; Abadie, C.; Huang, B. Development of Waste Tire Modified Concrete. *Cem. Concr. Res.* **2004**, *34* (12), 2283–2289. https://doi.org/10.1016/j.cemconres.2004.04.013.

(36) Roy, C.; Darmstadt, H. Carbon Blacks Recovered from Rubber Waste by Vacuum Pyrolysis - Comparison with Commercial Grades. *Plast. Rubber Compos. Process. Appl.* **1998**, *27* (7), 341–345.

(37) Martínez, J. D.; Cardona-Uribe, N.; Murillo, R.; García, T.; López, J. M. Carbon Black Recovery from Waste Tire Pyrolysis by Demineralization: Production and Application in Rubber Compounding. *Waste Manag.* **2019**, *85*, 574–584. https://doi.org/10.1016/j.wasman.2019.01.016.

(38) Wei, J.; Gong, Y.; Guo, Q.; Ding, L.; Wang, F.; Yu, G. Physicochemical Evolution during Rice Straw and Coal Co-Pyrolysis and Its Effect on Co-Gasification Reactivity. *Bioresour. Technol.* **2017**, *227*, 345–352. https://doi.org/10.1016/J.BIORTECH.2016.12.068.

(39) Wei, J.; Guo, Q.; Gong, Y.; Ding, L.; Yu, G. Synergistic Effect on Co-Gasification Reactivity of Biomass-Petroleum Coke Blended Char. *Bioresour. Technol.* **2017**, *234*, 33–39. https://doi.org/10.1016/J.BIORTECH.2017.03.010.

(40) Ding, L.; Zhou, Z.; Guo, Q.; Wang, Y.; Yu, G. In Situ Analysis and Mechanism Study of Char-Ash/Slag Transition in Pulverized Coal Gasification. *Energy and Fuels* **2015**, *29* (6), 3532–3544. https://doi.org/10.1021/acs.energyfuels.5b00322.

(41) Sánchez-Olmos, L. A.; Medina-Valtierra, J.; Sathish-Kumar, K.; Sánchez Cardenas, M. Sulfonated Char from Waste Tire Rubber Used as Strong Acid Catalyst for Biodiesel Production. *Environ.*

Prog. Sustain. Energy **2017**, *36* (2), 619–626. https://doi.org/10.1002/ep.12499.

(42) Liu, Z.; Wang, G.; Zhang, J.; Lee, J. Y.; Wang, H.; Sun, M.; Wang, C. Study on CO2 Gasification Reactivity and Structure Characteristics of Carbonaceous Materials from the Corex Furnace. *Energy and Fuels* **2018**, *32* (5), 6155–6166. https://doi.org/10.1021/acs.energyfuels.8b00072.

(43) Gil, M. V.; Riaza, J.; Álvarez, L.; Pevida, C.; Rubiera, F. Biomass Devolatilization at High Temperature under N2 and CO2: Char Morphology and Reactivity. *Energy* **2015**, *91*, 655–662. https://doi.org/10.1016/J.ENERGY.2015.08.074.

(44) Ding, L.; Gong, Y.; Wang, Y.; Wang, F.; Yu, G. Characterisation of the Morphological Changes and Interactions in Char, Slag and Ash during CO2 Gasification of Rice Straw and Lignite. *Appl. Energy* **2017**, *195*, 713–724. https://doi.org/10.1016/J.APENERGY.2017.03.098.

(45) Trubetskaya, A.; Surup, G.; Shapiro, A.; Bates, R. B. Modeling the Influence of Potassium Content and Heating Rate on Biomass Pyrolysis. *Appl. Energy* **2017**. https://doi.org/10.1016/j.apenergy.2017.03.009.

(46) Trubetskaya, A.; Jensen, P. A.; Jensen, A. D.; Steibel, M.; Spliethoff, H.; Glarborg, P.; Larsen, F. H. Comparison of High Temperature Chars of Wheat Straw and Rice Husk with Respect to Chemistry, Morphology and Reactivity. *Biomass and Bioenergy* **2016**. https://doi.org/10.1016/j.biombioe.2016.01.017.

(47) Zhang, Z. H.; Song, Q.; Yao, Q.; Yang, R. M. Influence of the Atmosphere on the Transformation of Alkali and Alkaline Earth Metallic Species during Rice Straw Thermal Conversion. *Energy and Fuels* **2012**, *26* (3), 1892–1899. https://doi.org/10.1021/ef2011645.